

Anti-Bcl-2 family members, zfBcl-x_L and zfMcl-1a, prevent cytochrome *c* release from cells undergoing betanodavirus-induced secondary necrotic cell death

Shi-Ping Chen · Jen-Leih Wu · Yu-Chin Su ·
Jiann-Ruey Hong

Published online: 24 January 2007
© Springer Science + Business Media, LLC 2007

Abstract Nervous necrosis virus (NNV)-induced, host cell apoptosis mediates secondary necrosis by an ill-understood process. In this study, redspotted grouper nervous necrosis virus (RGNNV) is shown to induce mitochondria-mediated necrotic cell death in GL-av cells (fish cells) *via* cytochrome *c* release, and anti-apoptotic proteins are shown to protect these cells from death. Western blots revealed that cytochrome *c* release coincided with disruption of mitochondrial ultrastructure and preceded necrosis, but did not correlate with caspases activation. To identify the mediator(s) of this necrotic process, a protein synthesis inhibitor (cycloheximide; CHX; 0.33 μg/ml) was used to block cytochrome *c* release as well as PS exposure and mitochondrial membrane permeability transition pore (MMP) loss. CHX (0.33 μg/ml) completely blocked viral protein B2 expression, and partly blocked protein A, protein α, and a pro-apoptotic death protein (Bad)

expression. Overexpression of *B2* gene increased necrotic-like cell death up to 30% at 48 h post-transfection, suggesting that newly synthesized protein (B2) may be involved in this necrotic process. Finally, necrotic death was prevented by overexpression of Bcl-2 family proteins, zfBcl-x_L and xfMcl-1a. Thus, new protein synthesis and release of cytochrome *c* are required for RGNNV-induced necrotic cell death, which can be blocked by anti-apoptotic Bcl-2 members.

Keywords Apoptosis · Betanodavirus · Cytochrome *c* · Mitochondria · Secondary necrosis · zfBcl-x_L

Introduction

Apoptosis is a genetically controlled event with roles in tissue development, homeostasis, and disease. Apoptosis and necrosis are two stereotyped mechanisms by which nucleated eukaryotic cells die [1–4]. Necrosis is considered to be a pathological reaction that occurs in response to major perturbations in the cellular environment such as a lytic viral infection. On the other hand, apoptosis is considered a physiological process that is part of homeostatic regulation during normal tissue turnover [1, 2].

Apoptosis is controlled at the mitochondrial level by sequestration of a series of apoptogenic proteins (such as cytochrome *c*, Smac/DIABLO, apoptosis inducing factor, and endonuclease G) in the mitochondrial intermembrane space, and cytosolic release of these factors on exposure to proapoptotic signals [5]. Mitochondria membrane permeabilization (MMP), which can be both inner and outer membrane permeabilization, precedes the signs of necrotic or apoptotic cell death, such as apoptosis-specific activation of caspases

J.-L. Wu and J.-R. Hong contributed equally to the research.

S.-P. Chen · Y.-C. Su · J.-R. Hong (✉)
Laboratory of Molecular Virology and Biotechnology,
Institute of Biotechnology, National Cheng Kung University,
Tainan 701, Taiwan
e-mail: jrhong@mail.ncku.edu.tw

S.-P. Chen
Taipei City Hospital, Yangming Branch,
Taipei, Taiwan

S.-P. Chen · J.-R. Hong
Research Center of Ocean Environment and Technology,
National Cheng-Kung University,
Tainan 701, Taiwan

J.-L. Wu
Laboratory of Marine Molecular Biology and Biotechnology,
Institute of Cellular and Organismic Biology, Academia Sinica,
Nankang, Taipei 115, Taiwan

[6]. Hence, the mitochondrion is regarded as a central integrator of pro-death stimuli, combining various types of proapoptotic signals into a common caspase-dependent pathway [5]. This pathway depends on the release of cytochrome *c* from mitochondria into the cytosol. This process is initiated by the interaction of mitochondria with one or more of the Bcl-2 family proteins. Thus, those Bcl-2 family proteins that are critical regulators of apoptosis act before cellular constituents are irreversibly damaged [7]. The Bcl-2 family of homologous proteins comprises pro-apoptotic (Bad, Bak, and Bax) as well as anti-apoptotic molecules (Bcl-2 and Bcl-x_L) [8, 9]. Their anti- or pro-apoptotic functions are heterodimer-dependent [8]. Furthermore, the ratio of anti-apoptotic to pro-apoptotic proteins also determines, at least in part, how a cell responds to apoptotic or survival signals [10]. Little is known about whether Bcl-2 family proteins can enhance resistance to aquatic virus-induced apoptotic cell death.

The family Nodaviridae contains two genera. Betanodaviruses predominantly infect fish, while alphanodaviruses mostly infect insects [11, 12]. Nodaviruses are small, non-enveloped, spherical viruses with bipartite positive-sense RNA genomes that are capped but not polyadenylated [12]. The larger genomic segment, RNA1, is a component of the viral RNA-dependent RNA polymerase (RdRp) that encodes protein A [13]. The smaller genomic segment, RNA2, encodes a capsid protein [14]. Alphanodaviruses synthesize a sub-genomic RNA3 from the 3' terminus of RNA1, which encodes two small proteins B1 and B2 [12, 15, 16]. Two putative ORFs, one for protein B1 (111 amino acids) and one for protein B2 (75 amino acids), also exist. Recently, the B2 protein of the nodavirus, flock house virus (FHV), was shown to either inhibit the silencing of viral RNAs in *Drosophila* cells [17, 18], *Caenorhabditis elegans* [19], plant [20] and mammalian cells [21] or to enhance viral RNA accumulation [22] to prevent the degradation of mRNA specifically targeted by homologous siRNA constructs. On the other hand, betanodavirus B2 function similarly in fish cells [23] and HeLa cells [24].

Despite their severe economic impact on the aquaculture industry, betanodaviruses have not been well studied. Characterization of the viral molecular regulation processes should help clarify the mechanism(s) of viral pathogenesis and infection. In a previous study, we demonstrated that redspotted grouper nervous necrosis virus (RGNNV) can induce apoptosis before necrosis in the grouper liver cell line (GL-av), that the mitochondrial permeability transition pore inhibitor BKA blocks necrosis [25], and that overexpression of the Bcl-2 member protein zBcl-x_L increases cell viability [26]. In addition, the Singapore strain of greasy grouper nervous necrosis virus (GGNNV) RNA2 induces apoptosis and activates the death effector enzyme caspase-3 in SB cells [27].

So we were particularly interested in how necrotic death is regulated in GL-av cells infected by the TN1 strain of RGNNV. Thus, our purpose in the present study was to determine the regulatory mechanism of RGNNV induced necrosis.

Materials and methods

Cell culture and reagents

The grouper liver cell line (GL-av) was subcloned from grouper liver cell line (GL-a), which was obtained from Dr. Lang (Institute of Biotechnology, National Cheng-Kung University, Taiwan, ROC). The cell line was grown at 28°C in Leibovit's L-15 medium (GibcoBRL, Gaithersburg, MD, USA) supplemented with 5% fetal bovine serum and 25 µg/ml of gentamycin. Annexin V-FLUOS Staining Kit, Annexin-V-Alexa 568 Staining Kit, and *In Situ* Cell Death Detection Kit were purchased from Roche Diagnostics (Mannheim, Germany). Cycloheximide (CHX) was purchased from Sigma Chemical Co. (St. Louis, MO, USA). ECL Western blotting detection system Kit was purchased from Amersham (Piscataway, NJ, USA). Apoptosis Detection, Mitochondria BioAssay™ Kit was purchased from US-Biological (Jomar Diagnostics Pty. Ltd., Stepney, Australia).

Virus

Naturally infected red grouper larvae were collected in 2002 in the Tainan prefecture and used as the source of red spotted grouper nervous necrosis virus (RGNNV Tainan No. 1; RGNNV TN1). The virus was used to infect GL-av cells, purified as described by Mori [28], and stored at –80°C.

Annexin V-FLUOS staining or annexin-V-alexa 568 staining

An analysis of PS on the outer leaflet of apoptotic cell membranes was performed using annexin V-fluorescein and propidium iodide (PI) to distinguish between apoptotic and necrotic cells. The GL-av cells (10⁵ cells/ml) were cultured to monolayer confluence in 60-mm Petri dishes for 20 h and then rinsed twice with phosphate-buffered saline (PBS). These cells were infected with RGNNV or uninfected (at 28°C for 0, 12 h, 24 h, or 48 h in an incubator), or nontransfected or transfected with one of two plasmids (pCDNA3.1 or pCDNA3.1-B2 [RGNNV B2 accession number: AY842578]) in 60-mm Petri dishes (at 28°C for 0, 24 h and 48 h in an incubator), and then the medium was removed. The monolayers were washed with PBS, incubated with 100 µl of staining solution (annexin V-fluorescein in a HEPES buffer containing PI; Boehringer-Mannheim,

Mannheim, Germany) for 10–15 min, and evaluated by fluorescence microscopy (488-nm excitation and 515-nm long-pass filter for detection annexin V-fluorescein; 515-nm excitation and 595-nm long-pass filter for detection annexin V-Alexa 568) [29].

For flow cytometric analysis, early events associated (at 0 h, 24 h, and 48 h p.t.) with apoptosis were evaluated using the binding of Annexin V to detect the translocation of phosphatidylserine (PS) from the inner side to the outer leaflet of the plasma membrane on apoptotic cells. Briefly, GL-av cells were incubated with fluorescein isothiocyanate (FITC)-conjugated Annexin V according to the manufacturer's instructions (Boehringer-Mannheim, Mannheim, Germany). The fluorescence images were acquired rapidly in the presence of PI.

Flow cytometric analysis

Analyses of stained RGNNV-infected and uninfected GL-av cells were performed on a FACS Vantage cell sorter (Becton-Dickinson, San Jose, CA, USA). Images of PI red fluorescence and FITC green fluorescence were obtained using, respectively, a 650-nm long-pass filter and 530 bandpass filter (FACS Vantage; the higher PI fluorescence intensity allowing separation of altered cells, PI⁺, from intact cells, PI⁻). Each analysis was done on at least 10,000 cells gated in the region of the cells on the basis of light scatter properties. Fluorescence data were displayed on four-decade log scales [30].

Preparation of the cytosolic cytochrome *c*

The GL-av cells were cultured as above and infected as above for 0, 12 h, 24 h, and 48 h. The method of Shimizu et al. [31] with slight modification was used to isolate mitochondria. Briefly, GL-av cells (2×10^6) were washed with PBS and homogenized in 0.3-ml of mitochondria isolation buffer (0.35 M mannitol, 10 mM Hepes, 0.1% bovine serum albumin, pH 7.2) using a glass homogenizer. Unbroken cells and nuclei were pelleted by centrifugation ($600 \times g$ for 5 min at 4°C). The mitochondria pellet was isolated from centrifuged supernatant ($10,000 \times g$ for 10 min at 4°C) and the supernatant was collected and mixed with 25 μ l of $10 \times$ SDS sample buffer. Samples (50 μ l) were boiled and subjected to Western blot analysis.

Western blot analysis

The GL-av cells were cultured as above. Cells were infected with RGNNV TN1 (m.o.i. = 5; propagated and titrated in GF-1 cells with a TCID₅₀ of $10^8/0.1$ ml) for 0, 12 h, 24 h, and 48 h. At the end of each incubation time the culture medium was aspirated, the cells were washed

with PBS and then lysed in 0.3 ml of lysis buffer (10 mM Tris base, 20% glycerol, 10 mM sodium dodecyl sulfate [SDS], 2% β -mercaptoethanol [β -ME], pH 6.8). An aliquot of the lysate was used for the separation of proteins by SDS-polyacrylamide gel electrophoresis [32]. The gels were subjected to immunoblotting [33] with 1:3000 anti-cytochrome *c*, Bad, Bak, Bcl-2, actin, caspase-8, caspase-9, caspase-3, cytochrome *c* oxidase I, and EGFP monoclonal antibodies and then 1:10,000 peroxidase-labeled goat anti-mouse conjugate (Amersham Biosciences, Piscataway, NJ, USA); or the gels were subjected to immunoblotting with 1:1000 anti-RGNNV B2 polyclonal antibodies and then 1:5,000 peroxidase-labeled goat anti-rabbit conjugate. Binding detected by chemiluminescence was captured on Kodak XAR-5 films (Eastman Kodak, Rochester, NY, USA).

Immunoelectron microscopy

EGFP-GL-av cells were infected with RGNNV TN1 (m.o.i. = 5) or uninfected, harvested 48 h after infection, and then prepared for electron microscopy. Thin-section electron microscopy and immunogold labeling were carried out as described by McNulty et al. [34]. The grids were stained with EGFP-specific polyclonal antiserum (1:1000) and subsequently with 15-nm gold-labeled goat anti-rabbit immunoglobulin G conjugate (1:50).

Evaluation of mitochondrial membrane potential with a lipophilic cationic dye

For assessment of mitochondrial membrane potential ($\Delta\Psi_m$), RGNNV-infected GL-av cells were stained with a fluorescent lipophilic cationic reagent known as MitoCapture (provided in the Mitochondria BioAssay™ Kit). This dye was trapped in mitochondria with normal $\Delta\Psi_m$ and released from mitochondria with abnormal $\Delta\Psi_m$ into the cytosol, resulting in loss of fluorescence intensity. The cell preparation and virus infection conditions are described above. GL-av cells were pretreated with CHX (0.33 μ g/ml) for 2 h, infected with RGNNV (or not infected) at 28°C for 0 h, 12 h, 24 h, and 48 h in an incubator, and then their media removed. MitoCapture reagent (500 μ l) was added to each 60-mm Petri dish and the dishes were incubated (37°C, 15–20 min). The cells were immediately viewed under a fluorescence microscope using band-pass filters that detect fluorescein and rhodamine [25].

Cell counts

Both virus-infected GL-av and uninfected control cells were labeled with Annexin V-fluorescein and then the number of positive cells (per 200 cells) in each sample was counted under a fluorescence microscope equipped with a 488-nm

excitation and 515-nm long-pass filter. Results were all expressed as mean \pm SEM. Data were analyzed using either paired or unpaired Student *t* tests, as appropriate. A value of $p < 0.05$ was taken to represent a statistically significant difference between group mean values.

Stable cell lines

EGFP-producing, zfBcl-x_L-producing, and zfMcl-1a-producing cells were obtained by transfection of GL-av cells with either pEGFP-C1, pEGFP-Bcl-x_L, or pEGFP-Mcl-1a

vectors and selection using G418 (800 μ g/ml) [26]. In these vectors, transcription of insert sequences is driven by the immediate-early promoter of human cytomegalovirus. About 2.5–3 months were needed for selection, depending on the cell properties.

Quantification of cell viability

GL-av cells were pretreated with CHX (0.33 μ g/ml; 2 h) before virus infection. The RGNNV-infected and uninfected GL-av cells were incubated at 28°C for 0, 12 h, 24 h, and 48 h.

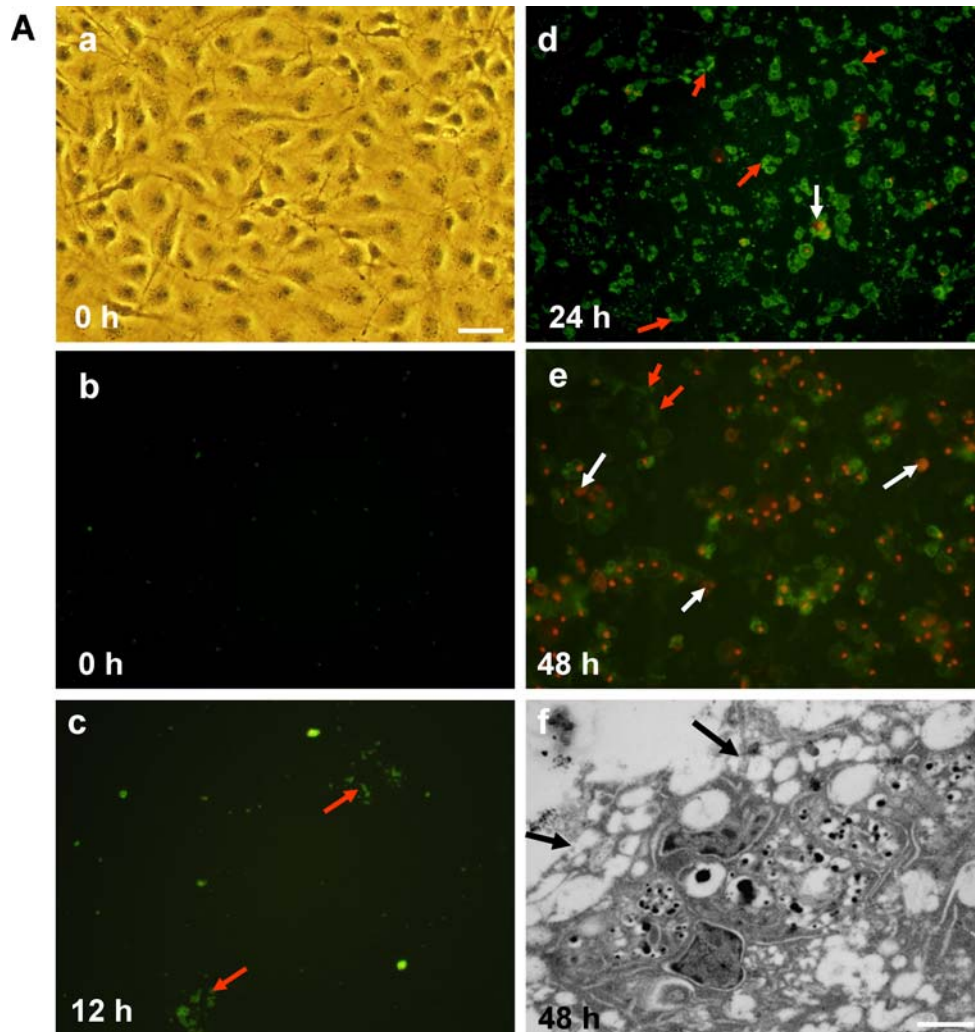


Fig. 1 Assessment of cytochrome *c* release from NNV-induced necrotic GL-av cells. (A) Phase-contrast fluorescence images of the early apoptotic and post-apoptotic necrotic RGNNV TN1-infected GL-av cells at 12 h, 24 h, and 48 h p.i. Annexin V-labeled early apoptotic cells are present at 12 h p.i. (Fig. 1(A):c; indicated by red arrows), and some necrotic cells (Fig. 1(A):d [24 h] and e [48 h]; indicated by white arrows) are fluorescently labeled. Normal control cells are shown in Fig. 1(A):a (phase-contrast image) and b (phase-contrast fluorescence image). (Bar) 10 μ m. Figure 1(A):f (immunoEM image) shows the breakdown of plasma membranes of post-apoptotic necrotic cells (indicated by black arrows). (B) Examples of flow cytometric profiles in

0 h (a) and (b) 48 h p.i. RGNNV-infected cells. PI/Annexin V-FITC dual staining fluorescence was measured from 10,000 cells. Numbers in the upper and lower right quadrants show late apoptotic/secondary necrotic (Annexin V⁺/PI⁺) cell percentages respectively. Viable cell percentage (Annexin V⁻/PI⁻) is shown in the lower left quadrant. (C) The release of cytochrome *c* in GL-av cells is shown 0, 24 h, and 48 h p.i. with RGNNV TN1 (m.o.i = 5). The release of cytochrome *c* from mitochondrial membranes was detected in gels using Western immunoblotting with polyclonal antibodies against mouse cytochrome *c* (Fig. (C):a). Internal control, cytochrome *c* oxidase I, is in Fig. (C):b

(Continued on next page.)

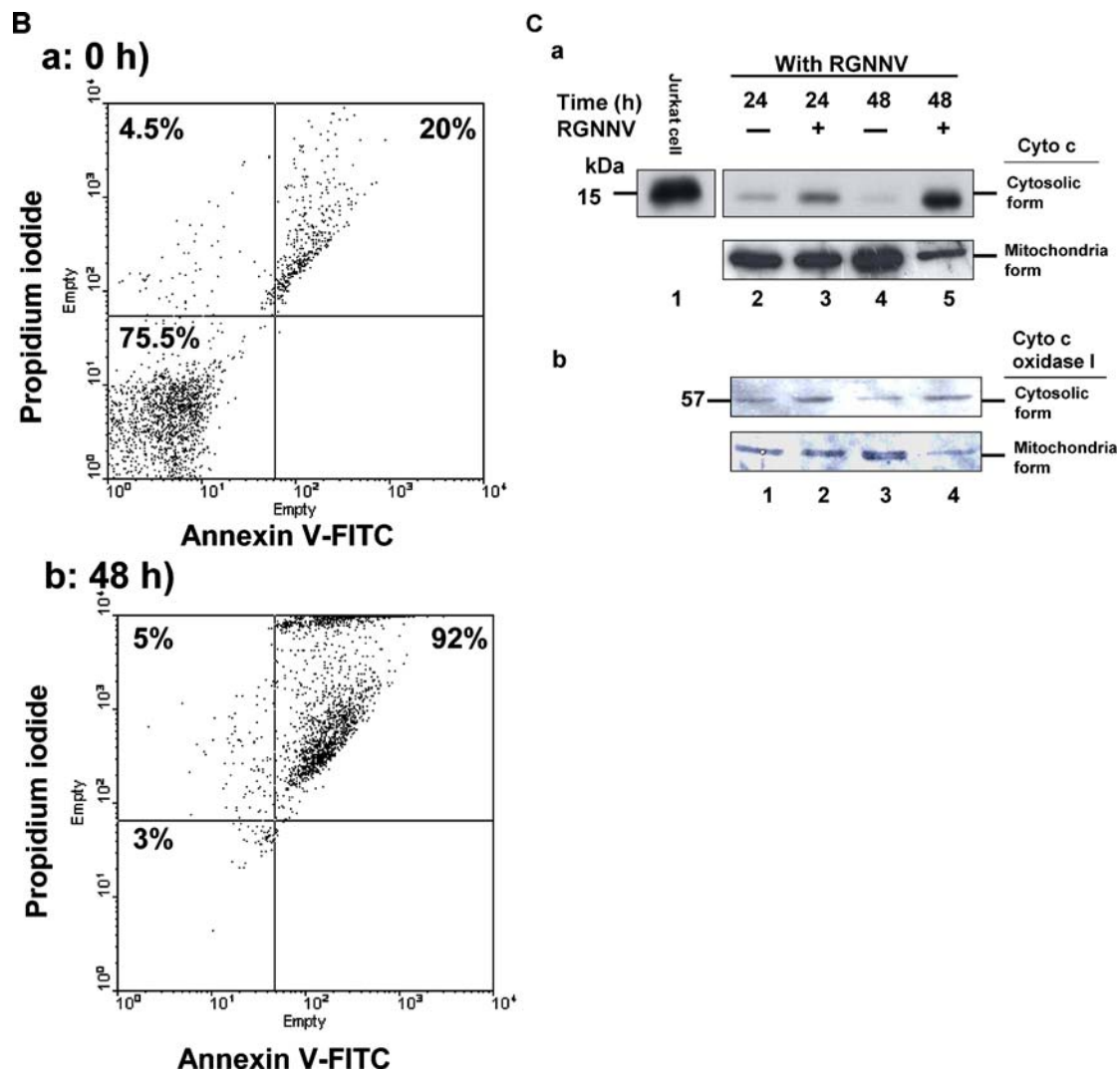


Fig. 1 (Continued).

About 10^5 EGFP, EGFP-Bcl- x_L , and EGFP-Mcl-1a GL-av cells/ml were cultured in 60-mm Petri dishes for 20 h. The RGNNV-infected EGFP-, EGFP-Bcl- x_L -, and EGFP-Mcl-1a-expressing GL-av cells (m.o.i. = 5) and uninfected cells were then incubated at 28°C for 0, 24 h, and 36 h. On the other hand, to assay blocking of cell death by pan-caspase inhibitor treatment, about 10^5 GL-av cells mL^{-1} were seeded per 60-mm Petri dish (Nunc) and cultured for 20 h. Then GL-av cells were pretreated with broad-spectrum caspase inhibitor (150 nM; zVAD-fmk) for 2 h and then infected with RGNNV (m.o.i. = 5) and incubated for 0, 12 h, 24 h, and 48 h at 28°C. At the end of each culture period, the cell layers were washed with PBS and treated with 0.1% trypsin-EDTA (0.5 ml, 1–2 min; Gibco, Grand Island, NY, USA). Cell viability was determined (in triplicate) using a trypan blue dye exclusion assay [35]. Each point represents the mean viability of three independent experiments \pm the standard error of the mean (SEM). Data were analyzed using

either paired or unpaired Student *t*-tests as appropriate. A value of $p < 0.05$ was taken to represent a statistically significant difference between mean values of groups.

Caspase activity assays

About 10^5 GL-av cells mL^{-1} were seeded in a 60-mm Petri dish (Nunc) and cultured for 20 h. Then GL-av cells were infected with RGNNV (m.o.i. = 5) and incubated for 0, 12 h, 24 h, and 48 h at 28°C. Caspase-8, -9, and -3 activation assays were performed using a kit (Clontech, Palo Alto, CA, USA). Experiments were performed using 1×10^6 cells/time point. Cells with caspase-8, -9, and -3 activation were centrifuged at $2000 \times g$, their supernatants were removed, and their cell pellets frozen at -70°C until all the different time points were collected. Assays were performed in 96-well plates and analyzed using a fluorescent plate reader (CytoFluor 4000, PerSeptive Biosystems, Framingham, MA,

USA). Cleavage of IETD-AFC, LEHD-AFC, and DEVD-AFC (synthetic caspase-8, -9, and -3 substrates) were used to determine caspase activity. Cleavage after the second Asp residue produces free AFC [28]. The amount of fluorescence detected is directly proportional to the amount of caspase-8, -9, and -3 activity. All the fluorogenic substrates assay experiments were performed at the same time, and both the mock and RGNNV-induced caspase-8, -9, and -3 activity profiles were the same in all experiments and are included in each figure to facilitate comparisons. Results of all experiments are reported as mean \pm S.E.M.

Results

RGNNV-induced apoptosis and transition to secondary necrosis is correlated with cytochrome *c* release in grouper liver cells

The feasibility of annexin V-fluorescein labeling and PI for the detection of early apoptotic and late necrotic cells was tested in GL-av cells. Figure 1(A) shows that PS from the intermembrane is exposed at 12 h p.i. (Fig. 1(A):c) and that this transposition changes postinfection morphology (Fig. 1(A), d [24 h p.i.] and e [48 h p.i.]). Distribution of the exposed PS is both random and concentrated (in Fig. 1(A):d and e; indicated by white arrows). A few necrotic cells (stained orange by PI; indicated by white arrow) can be seen at 24 h p.i. (Fig. 1(A):d), but necrotic cells predominate at 48 h p.i. (Fig. 1(A):e). The normal control (Fig. 1(A):a and b) cells stained by annexin V show patches of exposed PS at 0 h. Plasma membrane breakdown is apparent in necrotic cells (indicated by arrows; Fig. 1(A):f). Apoptotic cells in percent of total number (Fig. 1(B)) was 0.5 (0 h), 5 (12 h p.i.), 80 (24 h p.i.), and 14 (48 h p.i.). On the other hand, necrotic cells (in percent) gradually increased from 0.5 (0 h and 12 h p.i.) to 3 (24 h p.i.), and then markedly to 82 (48 h p.i.). Moreover, cytochrome *c* release from the mitochondrial membrane of infected cells increased threefold at 24 h (Fig. 1(C):a, lane 3) and tenfold at 48 h (Fig. 1(C):a, lane 5), and cytochrome *c* release from uninfected cells remained at basal level 24 h (lane 2) and 48 h (lane 4). Cytochrome *c* oxidase I release into cytosol (Fig. 1(C):b) was similar in infected cells between 24 h and 48 h (Fig. 1(C):b, lanes 2 and 4), but decreased slightly from the basal level in mock-infected control cells (Fig. 1(C):b, lanes 1 and 3).

Secondary necrotic cell death was coupled to infection-induced mitochondrial disruption

The GL-av-EGFP stable cell line was used to monitor mitochondrial morphology after RGNNV-infection. As apoptosis progressed to secondary necrosis (with DNA fragmentation

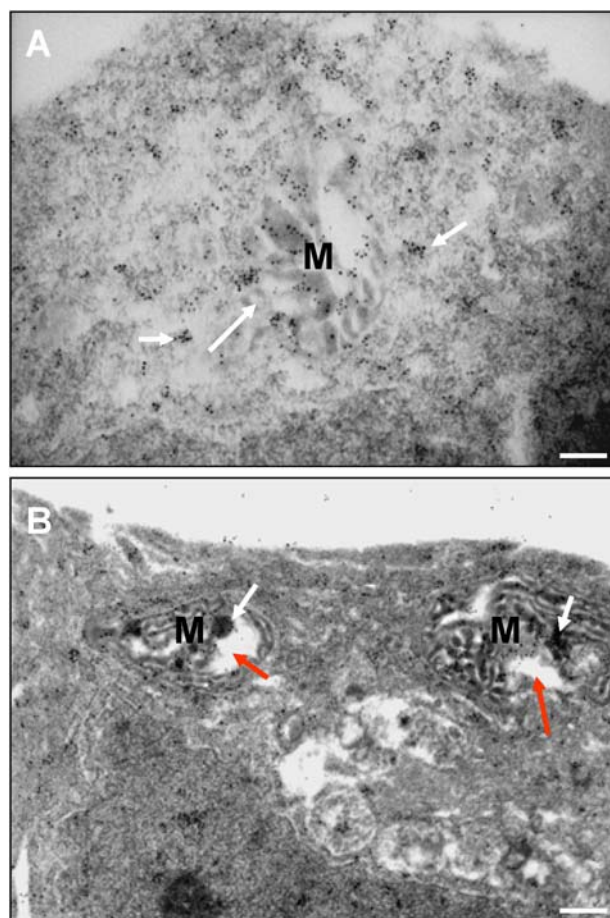


Fig. 2 Immunoelectron micrographs of ultrathin sections of GL-av-EGFP cells that were uninfected or infected with RGNNV TN1 strain and labeled with anti-GFP IgG. (A) EGFP is present (long white arrow) and forms small complexes (short white arrows) on normal GL-av-EGFP cells (the negative [M] control). (B) EGFP is present (small white arrows) on GL-av-EGFP cells infected with RGNNV TN1 (m.o.i. = 5) at 48 h p.i. Changes in mitochondrial ultrastructure indicative of efflux from the mitochondrial matrix (short red arrow) in the late apoptotic stage and indicative of mitochondrial breakdown (long red arrow) in the necrotic stage were observed. (Bar) 0.2 μ m

and finally cell disruption at 48 h p.i.), mitochondria became swollen (long red arrow; Fig. 2(B)) and severely damaged (short red arrow), permitting leakage from the mitochondrial matrix, in contrast to normal uninfected cells (long arrow; Fig. 1(A)). Interestingly, EGFPs formed small complexes (indicated by short arrow; Fig. 2(A)) in the cytoplasm and mitochondria of normal uninfected cells, but not of necrotic cells (Fig. 2(B)).

The protein synthesis inhibitor CHX inhibited PS exposure and loss of mitochondrial membrane potential (MMP) in GL-av cells

The ability of CHX to inhibit PS exposure in RGNNV-infected GL-av cells was tested. CHX (0.33 μ g/ml)

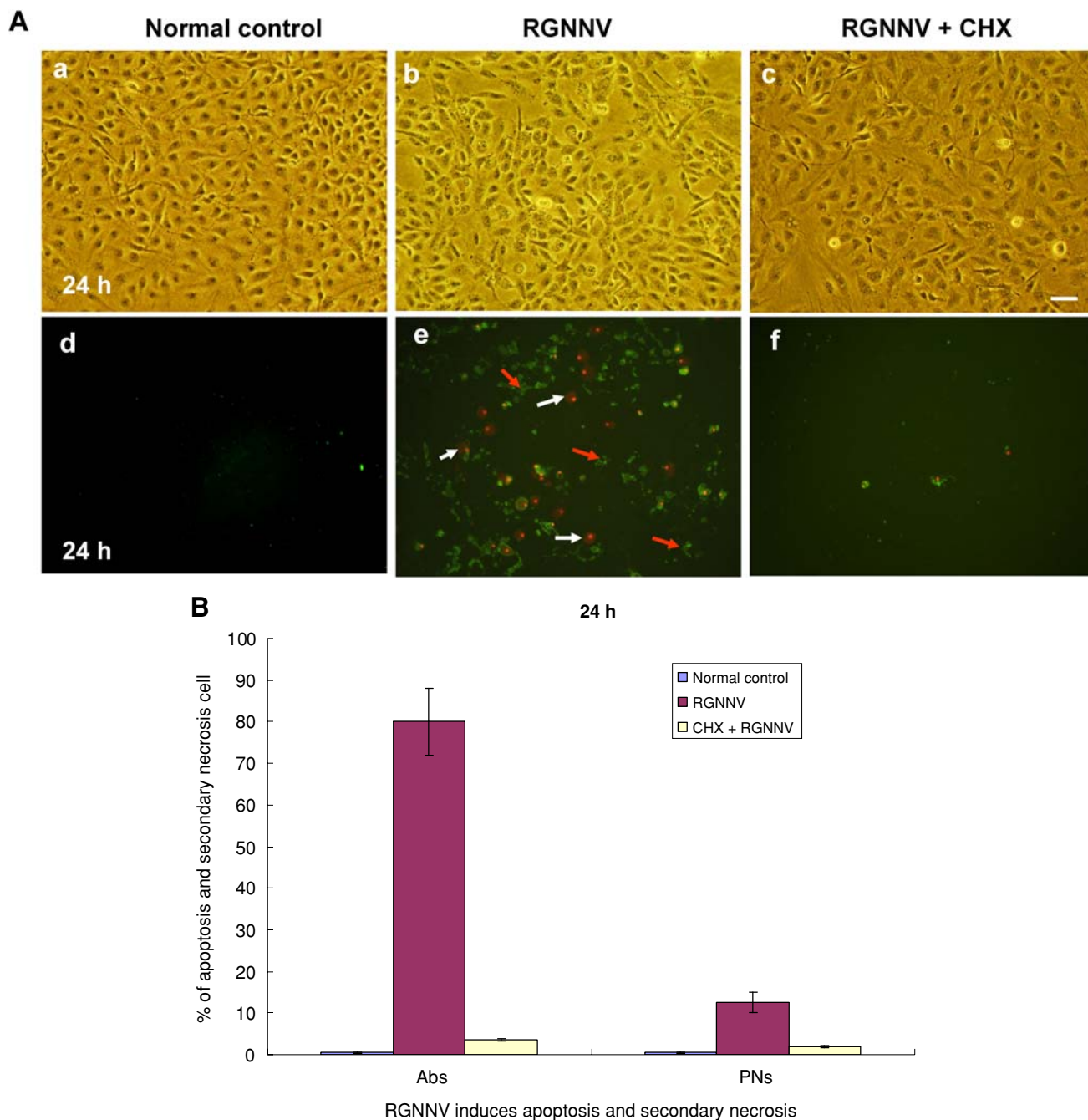


Fig. 3 Inhibition of protein synthesis blocked RGNNV-induced necrotic cell death. (A) Phase-contrast fluorescence image of GL-av cells treated with protein synthesis inhibitor CHX (0.33 μg/ml) for 2 h and then infected or not infected with RGNNV TN1 (m.o.i. = 5), at 24 h p.i. Phase-contrast fluorescence images (3A:d–f) show Annexin V-labeled early apoptotic cells (indicated by red arrows) and phase-contrast images (3A:a–c) show post-apoptotic necrotic cells (indicated

by white arrows). (B) The percent of viable GL-av cells treated with CHX (0.33 μg/ml) for 2 h and then infected or not infected (m.o.i. = 5) after 0, 24 h, and 48 h p.i. at 28°C. The cell viability of GL-av cells at each time point for each cell line was determined in triplicate; each point represents the mean viability in three independent experiments (± SEM)

effectively prevented PS exposure at 24 h p.i. (indicated by arrows; Fig. 3(A):c and f; compare infected cells (Fig. 3(A):b and e) with noninfected cells (Fig. 3(A):a and d)). CHX treatment effectively blocked entry into early apoptosis (apoptotic cells reduced from 78% to 2% and

secondary necrotic cells reduced from 12% to 3%); by contrast, apoptotic and necrotic cell levels in uninfected cell cultures remained 0.5%, respectively.

Mitochondrial function was evaluated using MitoCapture Reagent (Apoptosis Detection, Mitochondria BioAssay™

Kit), which contains PI and a lipophilic cationic dye. The latter fluoresces differently in healthy cells (where it aggregates into a fluorescent red polymer within mitochondria) and apoptotic cells (where it remains a fluorescent green monomer in cytoplasm because it cannot aggregate in mitochondria). CHX (0.33 $\mu\text{g}/\text{ml}$) inhibition of new protein synthesis was especially effective in preventing MMP loss at 48 h p.i. (indicated by arrows; Fig. 4(A):g–i; compare infected [Fig. 4(A):d–f] with uninfected cells [Fig. 4(A):a–c]). MMP loss occurred in 2.5% (12 h), 15% (24 h), and 93% (48 h) of infected cells p.i., whereas it only occurred in 1% (12 h), 3% (24 h), and 5% (48 h) of CHX-treated infected cells p.i. In uninfected cells, MMP loss occurred in less than 1% at 12 h,

24 h, and 48 h (Fig. 4(B)). Whether CHX treatment blocks cytochrome *c* release in the early or late apoptotic stages was determined. Figure 4(C) shows that the cytochrome *c* release was blocked either at 24 h p.i. (Fig. 4(C):a, lane 1) or 48 h p.i. (Fig. 4(C):a, lane 3; compare with RGNNV-infected cells without pretreatment (Fig. 4(C):a, lanes 2 and 4); β -actin, internal control (Fig. 4(C):b)). Finally, RGNNV was found to co-induce loss of MMP and cell viability (Fig. 4(D)). CHX prevented the loss of cell viability in infected cells (72% [24 h p.i.] and 12% [48 h p.i.] without CHX pretreatment *versus* 101% [24 h p.i.] and 102% [48 h p.i.] with CHX pretreatment). Normal uninfected cells remained fully viable at 0 h (100%), 24 h (118%), and 48 h (122%).

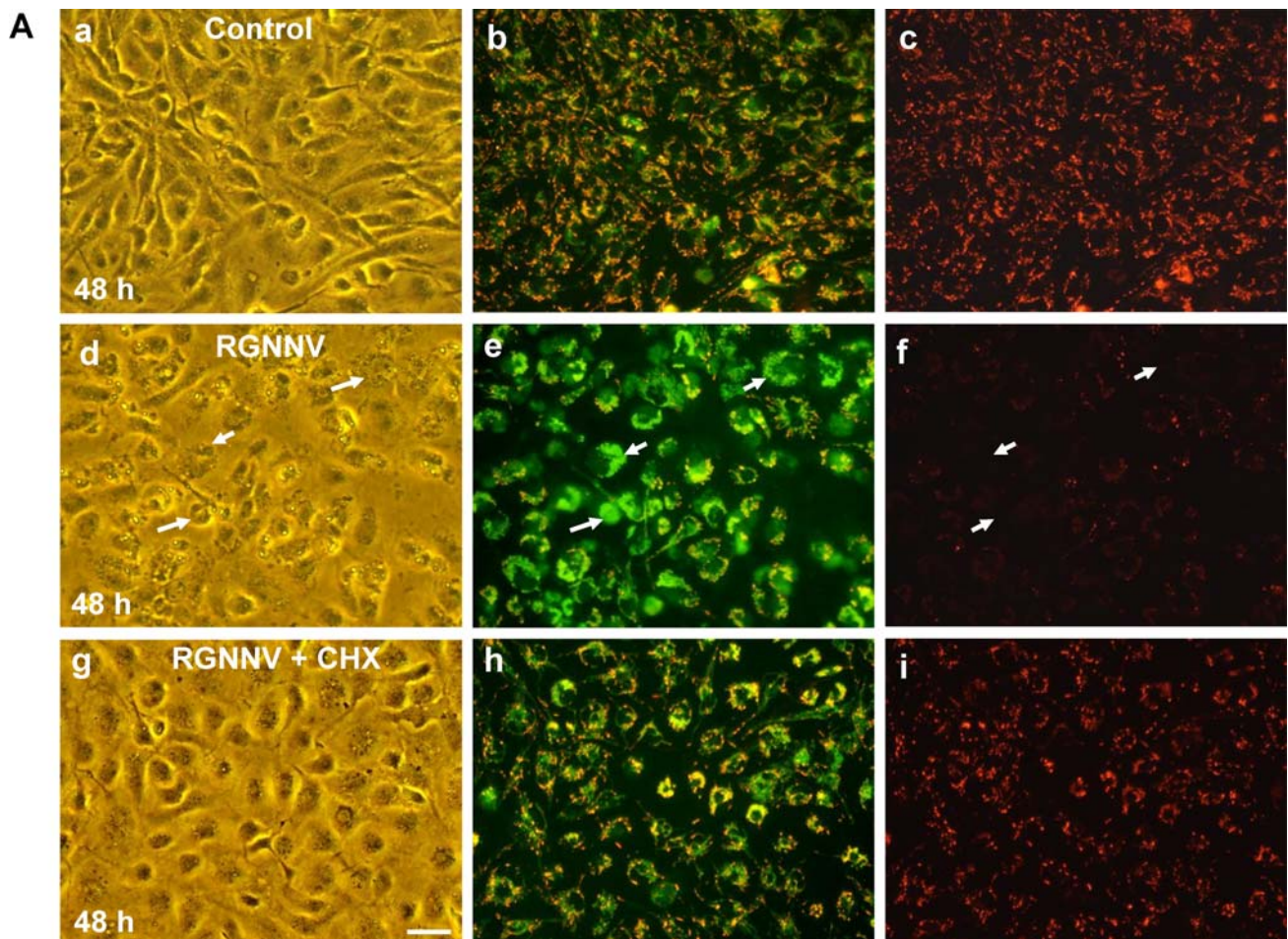
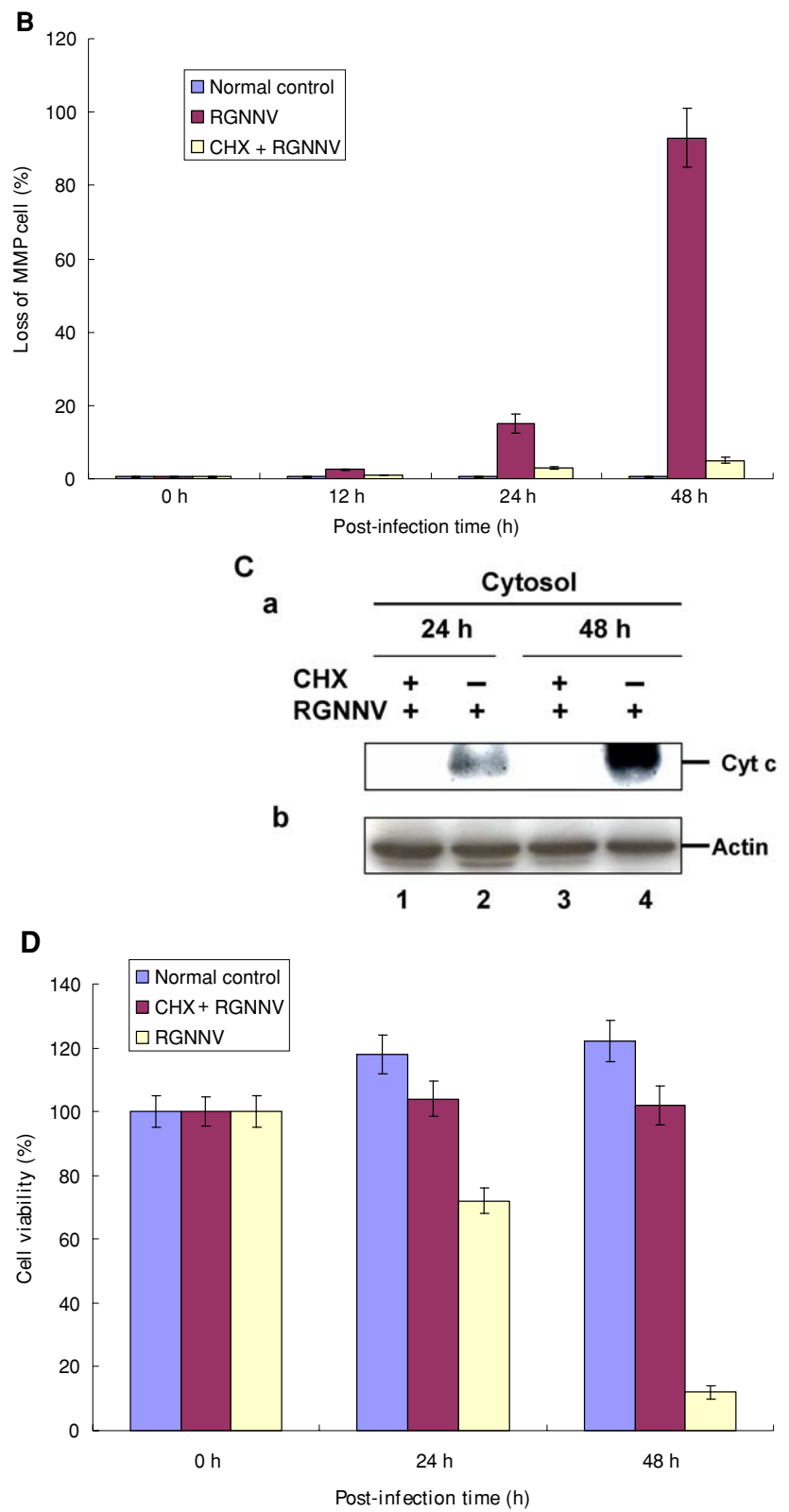


Fig. 4 Inhibition of protein synthesis blocks RGNNV-induced loss of MTP and cytochrome *c* release in necrotic cells. (A) CHX prevented loss of mitochondrial membrane potential at 48 h p.i. Fig. 4(A): d–f shows cells not pretreated with CHX and after RGNNV infection; Fig. 4(A):g–i shows cells both pretreated and infected; and Fig. 4(A):a–c shows cells both pretreated and mock-infected. Loss of mitochondrial membrane potential is indicated by arrows in Fig. 4(A): d–f. (Bar) 20 μm . (B) In infected cells, CHX prevented loss of mitochondrial membrane potential and cell viability at 0, 12 h, 24 h, and 48 h p.i. Viability at each time point was determined in triplicate; each point represents the mean viability in three independent experiments

(\pm SEM). (C) CHX prevented the release of cytochrome *c* in GL-av cells 24 h and 48 h p.i. with RGNNV TN1. The release of cytochrome *c* from mitochondrial membranes was detected by immunoblotting using polyclonal antibodies against mouse cytochrome *c* (C:a). Internal control is actin (C:b). (D) In cells pretreated with CHX (0.33 $\mu\text{g}/\text{ml}$ for 2 h) and then infected with RGNNV TN1 (m.o.i. = 5) or mock-infected at 28°C, the percentage of apoptotic and post-apoptotic necrotic GL-av cells was determined at 24 h p.i. The percentage of apoptotic and post-apoptotic necrotic cells at each time point was determined in triplicate; each point represents the mean viability in three independent experiments (\pm SEM) (Continued on next page.)

Fig. 4 (Continued).



RGNNV induces cell death through caspase-independent death pathway in GL-av cells

The mitochondrion is a central integrator of pro-death stimuli, streamlining various types of proapoptotic signals into a common caspase-dependent pathway [5]. Recently, the dogma that caspase activation is essential for apoptosis has been challenged [36, 37]. So, we wanted to know what death pathway (either caspase-dependent or -independent) is NNV-induced. The activities of caspase-3, -8, and -9 were therefore assayed. Interestingly, the activity of caspase-3 was 20% higher in the control cells at 24 h (Fig. 5(C)) p.i. However, the

activities of caspase-8 and -9 at 12 h, 24 h, and 48 h p.i. were all lower in the control cells (Fig. 5(A)–(C)). The higher caspase activity at 24 h in the control cells may reflect the need for this caspase in cell proliferation [38, 39]. In addition, the precursor profile of the three caspases was examined by Western blot (Fig. 5(D)). Moreover, the ability of pan-caspase inhibitor (150 nM) to block necrotic cell death of infected cells was tested. Pan-caspase inhibitor did not prevent necrotic cell death either at 24 h (Fig. 5(F)) or at 48 h (Fig. 5(F) and (E):c) p.i. Rather, death was enhanced 4% (24 h p.i.) and 5% (48 h p.i.) when compared with NNV-infected cells (Fig. 5(E):b and (F)) and control cells (Fig. 5(E):a and (F)).

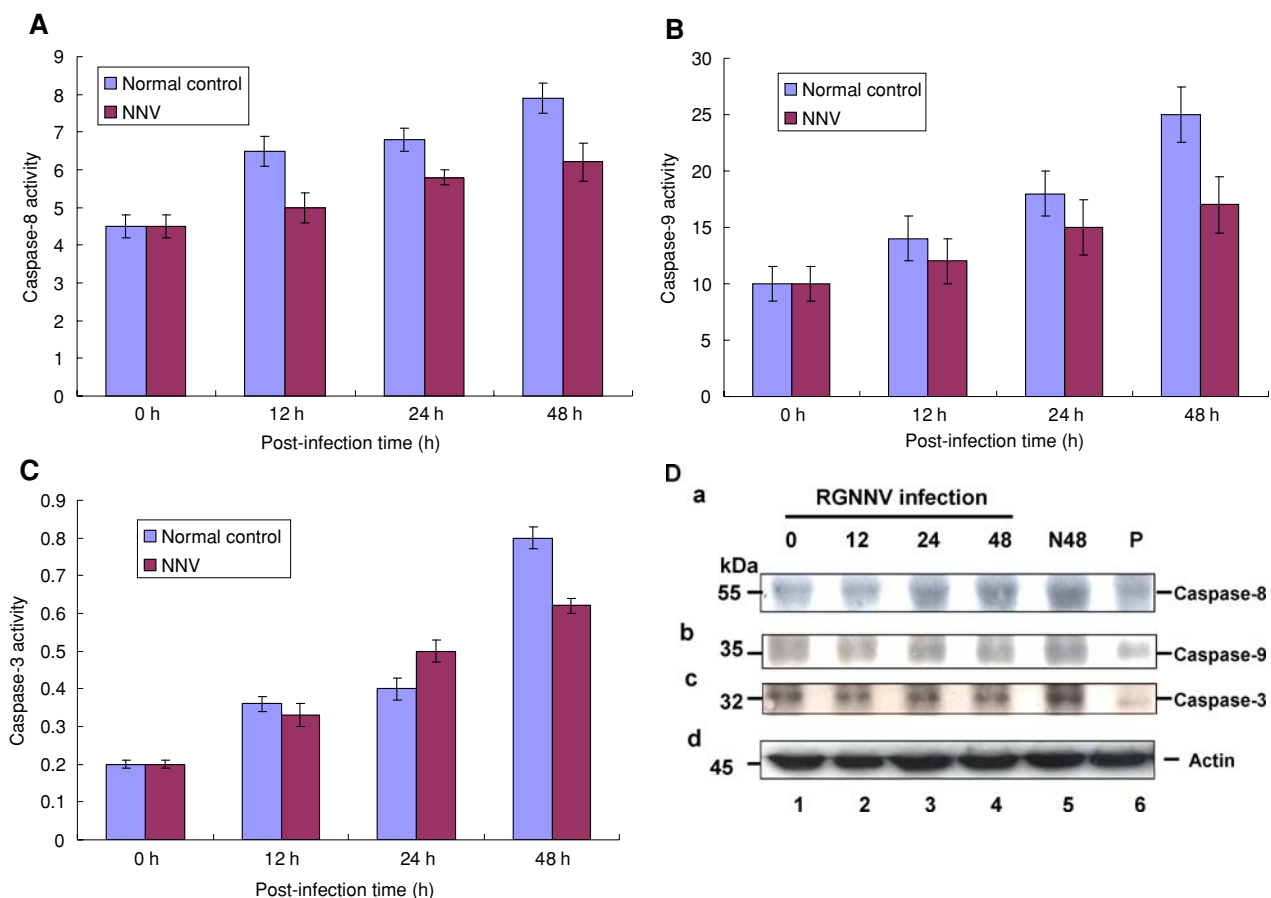


Fig. 5 Identification of RGNNV induces host cells through caspase-independent activation in GL-av cells. (A) Level of initiator caspase-8 activation at 0 h, 12 h, 24 h, and 48 h p.i. with RGNNV TN1. (B) Level of effector caspase-9 activation at 0 h, 12 h, 24 h, and 48 h p.i. with RGNNV TN1. (C) Level of effector caspase-3 activation at 0 h, 12 h, 24 h, and 48 h p.i. with RGNNV TN1. For Fig. 5(A)–(C), fluorogenic substrate assays were performed in triplicate. Error bars represent standard error of the mean. Fluorescence is expressed as arbitrary units. (D) Patterns of caspase precursors in GL-av cells following infection with RGNNV TN1 (m.o.i. = 5) for 0, 12 h, 24 h, and 48 h. Caspase-8 (D:a), -9 (D:b), and -3 (D:c) were detected by Western blots and gels were immunoblotted with polyclonal antibodies against

mouse immunoglobulins. (D:d) Internal control was actin in D:a–d. (E) Phase-contrast image of post-apoptotic necrotic RGNNV-infected GL-av cells pretreated (E:b) or not pretreated (E:c) with broad-spectrum caspase inhibitor (zVAD-fmk; 150 nM) for two hours before infection (m.o.i. = 5) at 48 h p.i. Post-apoptotic necrotic cells are present in E:b, c and d (enlarged micrograph from b) and indicated by arrows. (F) Viability (0, 24 h, and 48 h p.i.) of uninfected GL-av cells, GL-av cells infected with RGNNV (m.o.i. = 5) at 28°C, and infected GL-av cells pretreated with zVAD-fmk (150 nM) for two hours. Cell viability at each time point for each treatment was determined in triplicate; each point represents the mean viability in three independent experiments (\pm SEM) (Continued on next page.)

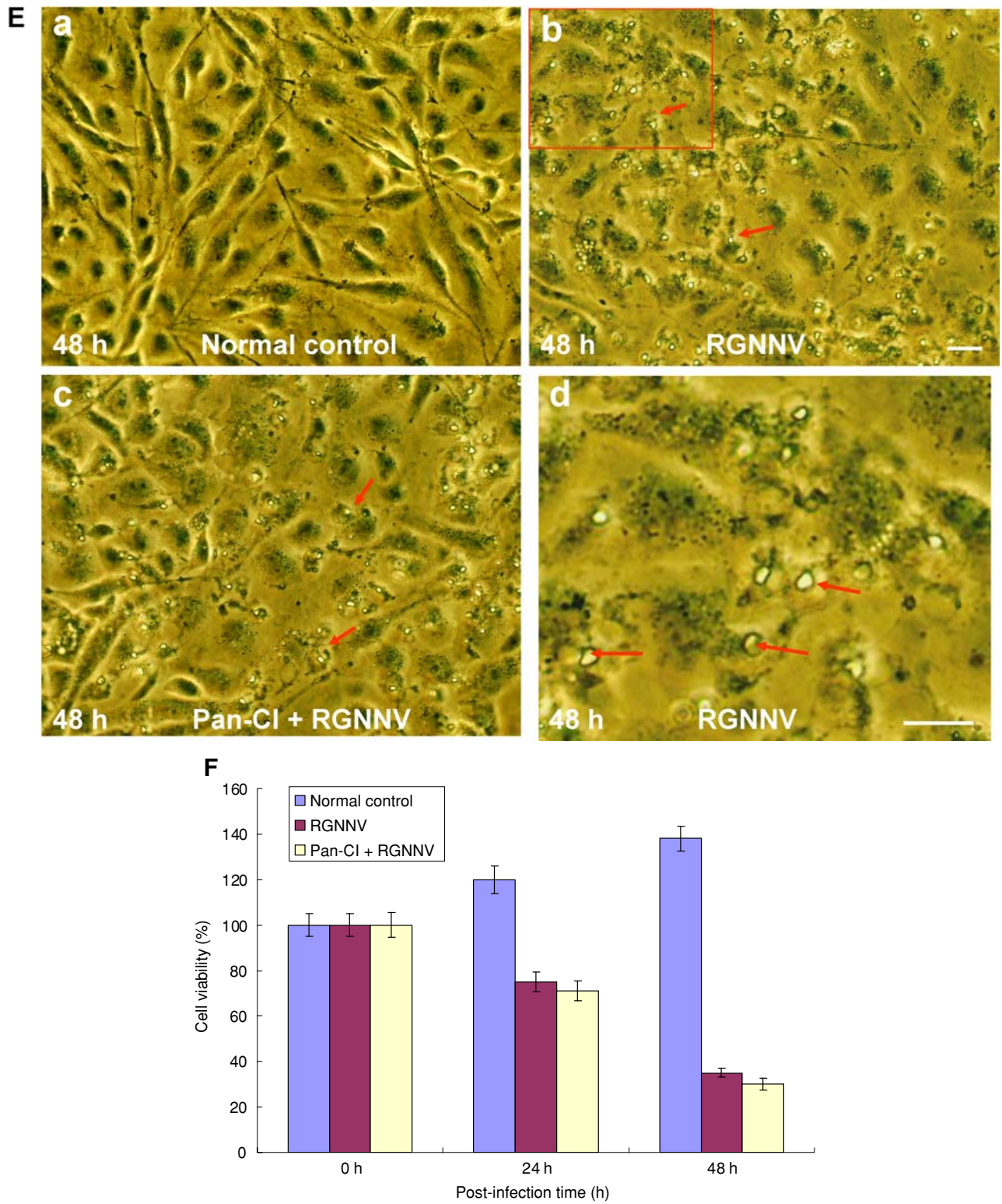


Fig. 5 (Continued).

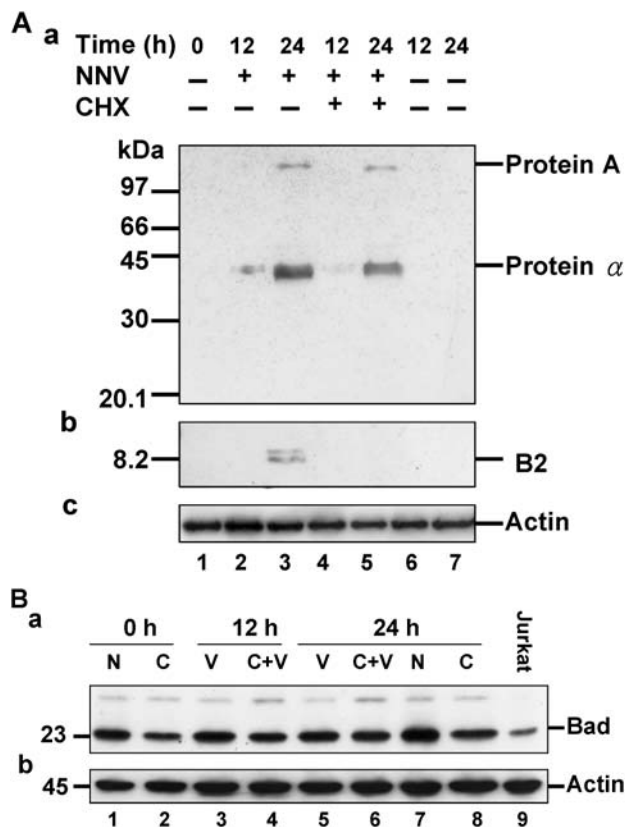


Fig. 6 CHX (0.33 $\mu\text{g/ml}$) blocked RGNNV viral protein expression and host cellular protein expression differently in GL-av cells. (A and B) Viral and cellular proteins were expressed in GL-av cells following infection with RGNNV TN1 (m.o.i. = 5) for 0, 12 h, and 24 h. RGNNV protein A (A:a), protein α (A:a), and non-structural protein B2 (A:b) were detected by immunoblotting using polyclonal antibodies against the whole RGNNV protein A and protein α , and polyclonal antibodies against the N-terminus peptide of B2. Internal control actin is shown in A:b and c. (B) Host cell protein expression in GL-av cells following infection with RGNNV for 0, 12 h, and 24 h. Bad was detected using immunoblotting with mouse monoclonal antibodies against Bad. Internal control actin is in B:b

The death mediator(s) may be a newly synthesized protein whose synthesis is blocked by CHX

The degree of protein inhibition by CHX (0.33 $\mu\text{g/ml}$) pretreatment for 2 h prior to infection depends on the particular viral protein. Expression of B2 protein (RNA3 coded protein) was completely inhibited (Fig. 6(A):b, lane 3 and 5) at 24 h p.i., whereas expression of protein A (RNA 1 coded protein; Fig. 6(A):a, lanes 3 and 5) was decreased only 10%, and expression of protein α (RNA2 coded protein; Fig. 6(A):a, lanes 2–5) decreased 40% at 12 h (lane 2 compared with lane 4) and 60% at 24 h (lane 4 compared with lane 5). The controls included mock-infected cells (Fig. 6(A):a, lanes 1, 6, and 7) and β -actin (internal control; Fig. 6(A):c). On the other hand, levels of pro-apoptotic proteins Bad (Fig. 6(B):a) did not in-

crease at 12 h and 24 h p.i. in infected cells pretreated with CHX when compared to uninfected (mock-infected) cells.

Anti-apoptotic Bcl-2 family proteins zfBcl-x_L and zfMcl-1a inhibit necrotic death

zfBcl-x_L and zfMcl-1a were tested to determine whether they can block the RGNNV-induced host necrotic cell death and enhance cell viability. The stable clones of zfBcl-x_L- and zfMcl-1a-producing GL-av cells were selected (Fig. 7(A)–(B)). Synthesis of EGFP (Fig. 7(A):a), EGFP-Mcl-1a (Fig. 7(A):b), and EGFP-Bcl-x_L (Fig. 7(A):c) proteins by their respective clones was confirmed using Western blots (Fig. 7(B)). To determine whether zfBcl-x_L and zfMcl-1a can block necrotic cell death of RGNNV-infected clones, PS export to the outer leaflet of the plasma membrane (a well-known early event in apoptosis) was used as a marker of post-apoptotic necrosis (Fig. 7(C)). Either zfBcl-x_L (Fig. 7(C):e and f) or zfMcl-1a (Fig. 7(C):g and h) blocked post-apoptotic necrosis (indicated by arrows; Fig. 7(C):c and d) at 36 h p.i. Mock-infected cells did not become necrotic (Fig. 7(C):a and b). The number of apoptotic cells (Abs) and post-apoptotic necrosis cells (PNs) was higher in RGNNV-infected cells (8% Abs and 96% PNs) than in the infected stable zfBcl-x_L clone (4% Abs, 6% PNs), infected stable zfMcl-1a clone (8% Abs, 3% PNs), and corresponding mock-infected cells (0.5% Abs, 0.5% PNs). Moreover, cell viability of both the infected zfBcl-x_L clone (100%, 102%, and 106%) and infected zfMcl-1a clone (100%, 101%, and 98%) was higher than that of the infected, original, noncloned GL-av cells (100%, 86%, and 4%) at 0, 24 h, and 36 h p.i., respectively. The viability of the corresponding mock-infected EGFP-, EGFP-Bcl-x_L- and EGFP-Mcl-1a-producing cells at 0 h (100%), 24 h (112%, 110%, and 113%, respectively), and 36 h (124%, 120% and 125%, respectively) was even higher (Fig. 7(D)).

Over-expression of RGNNV B2 induces necrotic-like cell death in GL-av cells

CHX treatment (0.33 $\mu\text{g/ml}$) completely blocked B2 protein expression and was used to determine whether B2 is a necrotic cell death inducer. Western blotting showed that B2 protein (8.5 kDa) is overexpressed in GL-av cells at 48 h p.t. (Fig. 8(A), lane 2). Annexin V-FITC staining found that B2 can apparently induce necrotic-like cell death (Fig. 8(B):c–d, phase-contrast micrographs; g–h, red fluorescent micrographs). Enlarged images (Fig. 8(B): i and j from Fig. 8(B):d and h, respectively) clearly show necrotic morphological changes (Fig. 8(B):f, indicated by arrows) under phase-contrast microscopy and necrotic cells with surface blebs (Fig. 8(B):h, indicated by arrows), which indicate the translocation of phosphatidylserine (PS) from the inner side

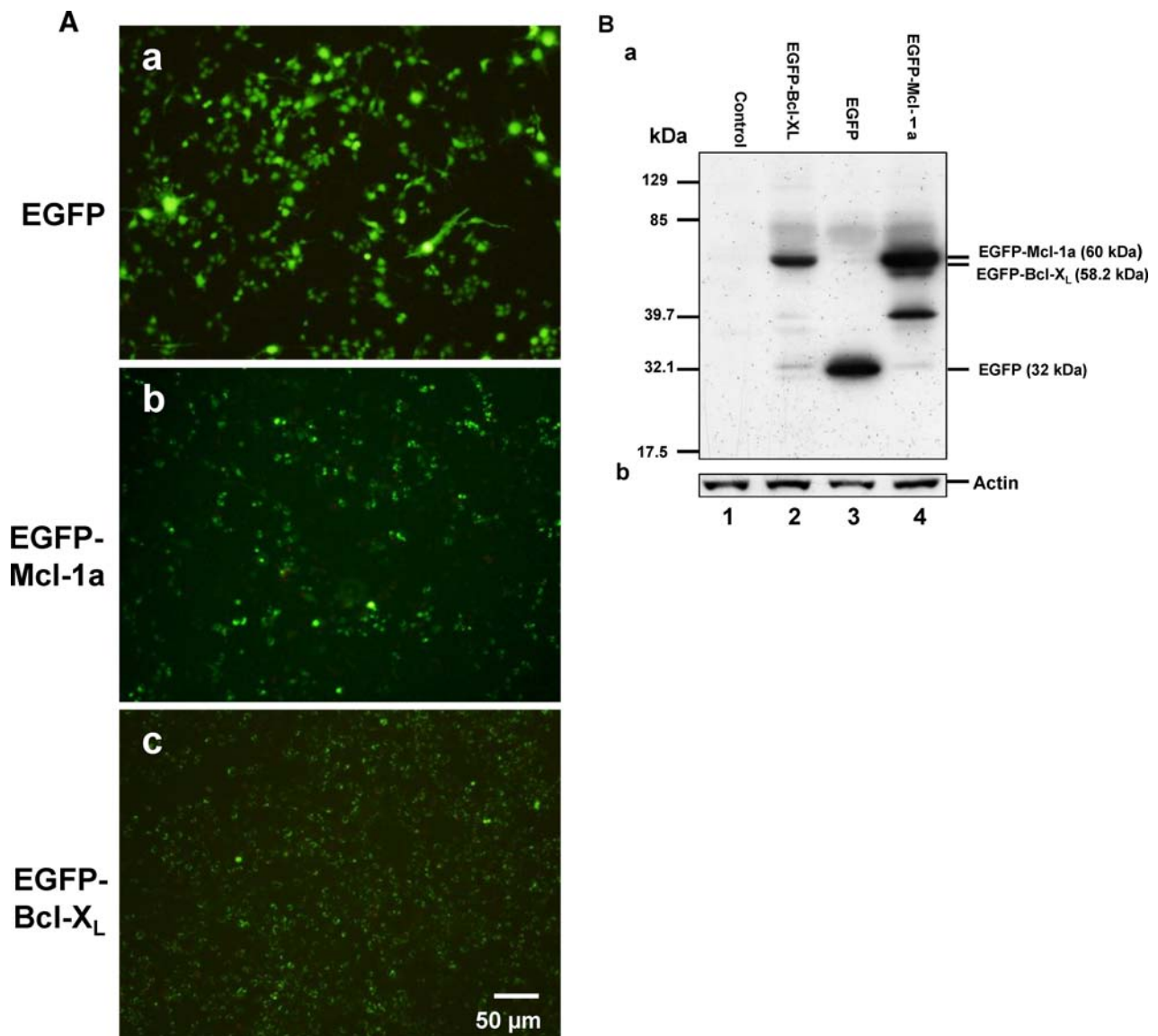


Fig. 7 Anti-apoptotic proteins zfBcl-x_L and zfMcl-1a prevented RGNNV-induced necrotic cell death. (A) Assessment of zfBcl-x_L, zfMcl-1a, and EGFP expression in stable GL-av cell lines. EGFP-producing (6A:a), zfBcl-x_L-producing (6A:b), and zfMcl-1a-producing (6A:c) cells were obtained by transfection of GL-av cells with a pEGFP-C1, pEGFP-Bcl-x_L, and pEGFP-Mcl-1a vectors and selection with G418 (800 μg/ml) for about 2.5–3 months. (Bar) 50 μm. (B) Stable clones of GL-av cells containing genes for EGFP, EGFP-Bcl-x_L, and EGFP-Mcl-1a were identified using Western blots. (B:a) The fusion protein of EGFP and zfBcl-x_L (lane 2), EGFP (lane 3), EGFP and zfMcl-1a fusion protein (lane 4), and the negative control (absence of either the EGFP, or the Bcl-2 proteins zfBcl-x_L or zfMcl-1a; lane 1) are shown. Internal control actin is in B:a and b. (C) Phase-contrast fluorescence image showing the morphology of post-apoptotic necrotic RGNNV-infected GL-av cells (m.o.i. = 5) cotransfected with plasmids containing EGFP, zfBcl-x_L, and zfMcl-1a at 36 h p.i. Post-apoptotic necrotic

cells are present (C:c and d). Phase-contrast fluorescence image (C:c and d) showing the morphology of Annexin V-labeled post-apoptotic necrotic cells either not transfected (C:e and f; indicated by arrows), or stably transfected with zfBcl-x_L-containing plasmids (C:g and h; indicated by arrows), zfMcl-1a-containing plasmids, or uninfected cells transfected with EGFP-containing plasmids (Fig. 6(C):a and b; indicated by arrows). (D) The percentage of apoptotic and post-apoptotic necrosis cells producing EGFP, zfBcl-x_L, and zfMcl-1a 36 h p.i. at 28°C with or without RGNNV TN1 (m.o.i. = 5). The percentages of apoptotic and post-apoptotic necrosis GL-av cells were determined at each time point in triplicate; each point represents the mean viability in three independent experiments. (E) The viability of EGFP-, zfBcl-x_L-, and zfMcl1a-producing GL-av cells infected with GRNNV TN1 (m.o.i. = 5) was determined at 0, 24 h, and 36 h p.i. in triplicate; each point represents the mean viability in three independent experiments (Continued on next page.)

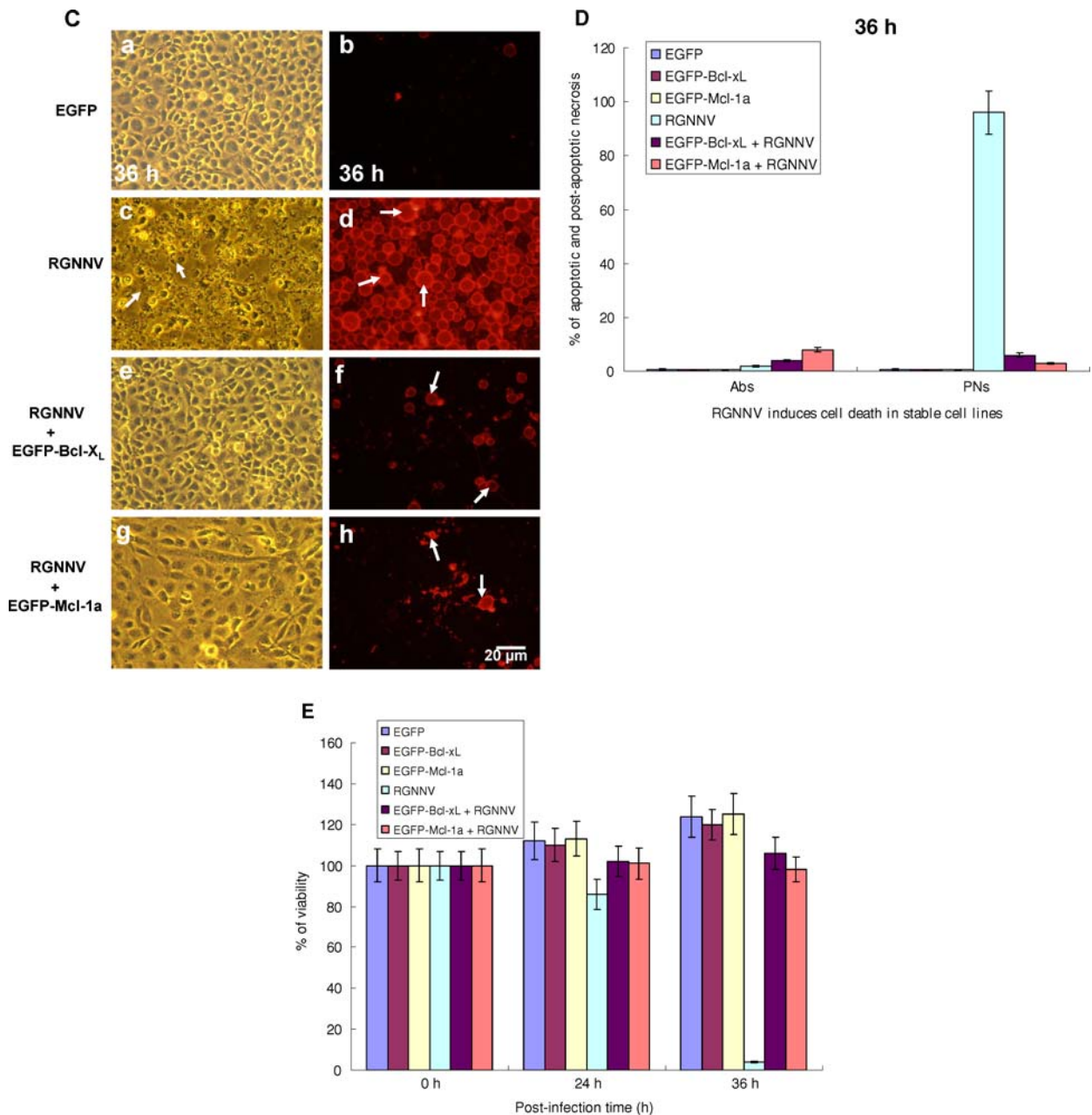


Fig. 7 (Continued).

to the outer leaflet of the plasma membrane on the apoptotic cells and necrotic cells. Moreover (Fig. 8(C)), more necrotic cells (1%, 10.5% and 30%) were induced by pCDNA3.2-B2 than pCDNA3.1 transfection (1%, 1.5% and 3%) at 0, 24 h, and 48 h p.t., respectively.

Discussion

Early during infection with RGNNV, fish swim abnormally (in circles or to the right), lie on their sides, or lie belly up.

Histopathological changes include extensive cellular vacuolation and necrotic neuronal degeneration in the central nervous system and retina [40]. How betanodavirus infection induces neuronal degeneration and whether neuronal degeneration causes abnormal swimming behavior remain unanswered questions. Previous studies showed that RGNNV infection induced post-apoptotic necrotic cell death and that ANT inhibitor BKA may inhibit the loss of mitochondrial membrane potential [25], but the triggering mechanism and downstream events after mitochondrial damage are still not delineated.

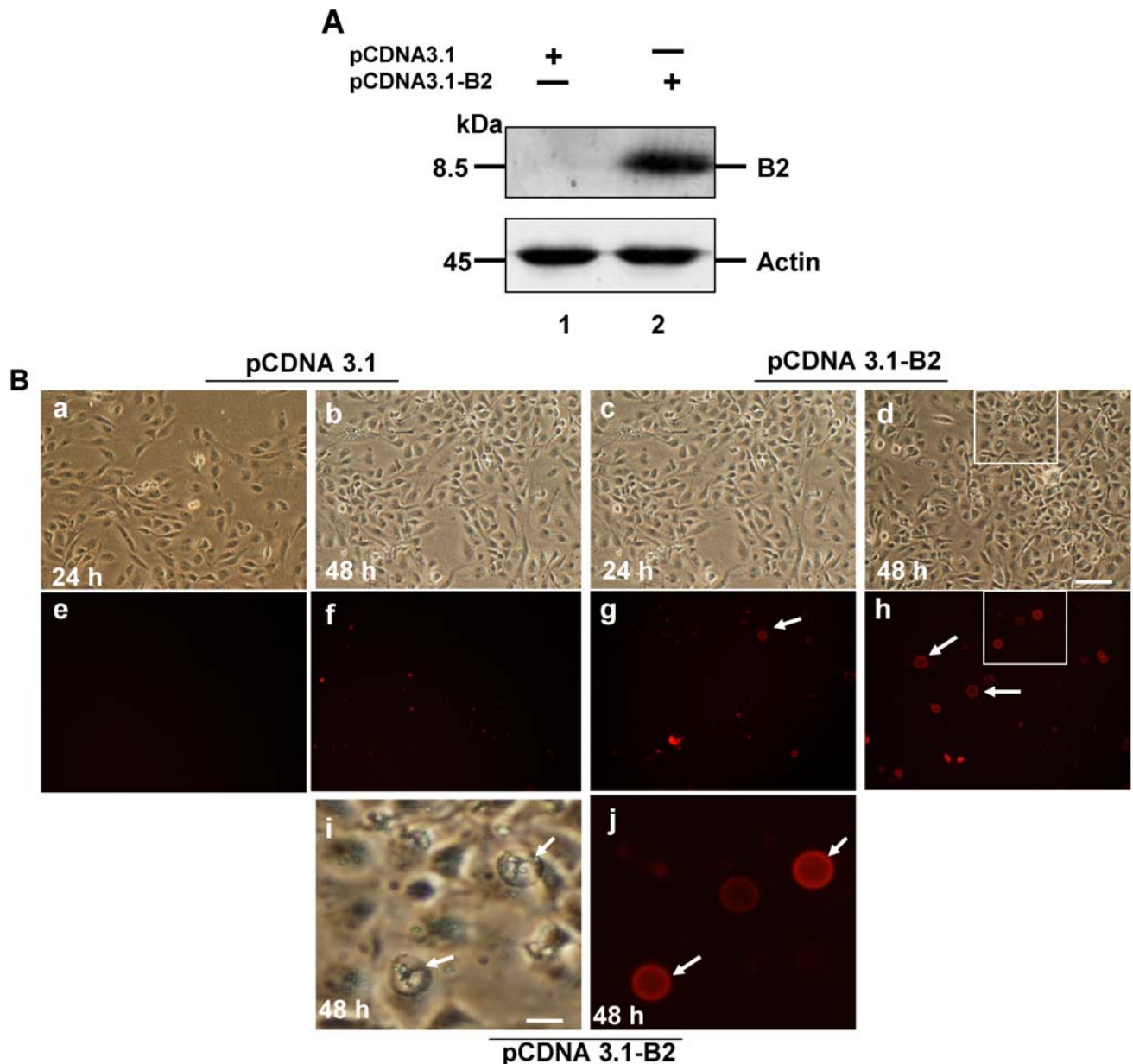


Fig. 8. Determination of whether B2 induces post-apoptotic necrotic cells in GL-av cells. (A) Western blot shows RGNNV B2 expression of pCDNA3.1 transfected GL-av cells (lane 1) and pCDNA3.1-B2 transfected GL-av cells (lane 2) at 48 h p.i. Actin is the internal control. (B) Phase-contrast fluorescence image demonstrates that B2 induced necrosis 24 h and 48 h p.i. with pCDNA3.1-B2. B2 induces necrotic-like cells are present (8B:c, d, g, h, i, and j; indicated by arrows). Vector

(pCDNA3.1) alone transfected GL-av cells are shown in 8B: b, e, and f. (C) The percentage of necrotic-like cells producing B2 at 0 h, 24 h, and 48 h p.i. The percentages of necrotic-like GL-av cells were determined at each time point in triplicate; each point represents the mean viability in three independent experiments

(Continued on next page.)

Cytochrome *c* release correlated with RGNNV-induced necrotic cell death

In our system, the transition from early apoptosis to necrosis was investigated. In particular, we tried to determine whether cytochrome *c* release was mediated through a caspase-dependent or -independent death pathway. Figure 1 shows that cytochrome *c* release began at 24 h p.i. (Fig. 1(C), lane 3),

and was largely complete at 48 h p.i. (Fig. 1(C), lane 5; compare with mock-infected cells at 24 h (Fig. 1(C), lane 2) and 48 h [Fig. 1(C), lane 4] p.i.). The course of cytochrome *c* release is correlated with that of necrotic cell death (see annexin V results [Fig. 1(A):c {24 h p.i.} and d {48 h p.i.}] and the percentage of necrotic cells [Fig. 1(B) showing marked increase from 3% {24 h p.i.} to 82% {48 h p.i.}]).

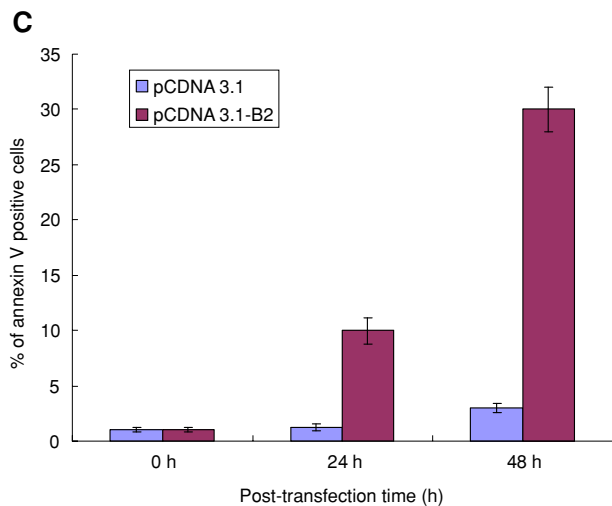


Fig. 8 (Continued).

The mitochondria are the central integrators of pro-death stimuli, combining various proapoptotic signals into a common caspase-dependent pathway [5], but some investigators no longer consider that caspase activation is a requirement for apoptosis [36, 37]. Our assay of caspase-3, -8, and -9 activities revealed no significant differences in the activities of caspases (Fig. 5A–C) between control cells and infected cells at 0, 24 h, 48 h, and 72 h p.i. and no blocking of activity by pan-caspase inhibitor (Fig. 5E). Our results suggest that whether betanodavirus induction is *via* a caspase-dependent or caspase-independent death pathway may depend on the cell line. In grouper liver cells, RGNNV infection induces *via* a caspase-independent death pathway, while in sea bass cells, GGNNV infection seems to induce *via* a caspase-dependent death pathway [27].

New synthesis of a death mediator(s) may trigger MMP loss

Interest in apoptosis has promoted a search for genes that encode apoptotic proteins. Subtractive hybridization studies of T cells suggest that a class of genes that induce RP-8 and PD-1 is transcribed after signals for apoptosis are initiated [41, 42], and treatment with cycloheximide (CHX) can block apoptosis in T cells. On the other hand, CHX treatment of CHSE-214 cells (a line derived from salmon) inhibits IPNV-induced apoptotic cell death by blocking expression of the pro-apoptotic gene Bad [29]. Persistent protein synthesis, which does not shut off gene expression [43], is believed to be a prerequisite for triggering necrotic cell death, but whether new protein synthesis is needed in this process is little known. In our system (i.e., GL-av cells pretreated with CHX [0.33 μ g/ml] and then infected with RGNNV TN1 strain), apoptotic and necrotic cell death were blocked (compare Fig. 3(A):f with Fig. 3(A):e) at 24 h p.i. CHX decreased

the percentage of apoptotic cells from 78% to 2% (Fig. 3(B)) and of necrotic cells from 12% to 3% (Fig. 3(B)) at 24 h p.i., reduced RGNNV-induced mitochondrial damage (compare Fig. 4(A):d–f with Fig. 4(A):g–i), blocked cytochrome *c* release at 24 h (Fig. 4(C): lane 1) and 48 h p.i. (Fig. 4(C): lane 3), and enhanced cell viability up to 29% (24 h) and 90% (48 h) when compared with the viability of untreated virus-infected cells. In addition, CHX blocked synthesis of the viral RNA3-encoded protein, B2, which may act as a suppressor of siRNA silencing [17–24], and overexpression of B2 was associated with post-apoptotic necrotic cell death (Fig. 8). Thus, the *B2* gene may be a necrotic death gene. Moreover, CHX only partially blocked the synthesis of capsid proteins (e.g., RNA 2-coded protein α), which may be a death inducer in SB cells [27], but in our system, blocking the synthesis of just half the capsid protein was sufficient to block necrotic cell death. On the other hand, over-expression of protein α induced apoptotic cell death in GL-av cells (data not shown).

The anti-apoptotic proteins zfBcl-x_L and zfMcl-1a may act as death regulators by preventing loss of MMP

The Bcl-2 family of proteins includes both anti- and proapoptotic molecules that control a critical, intracellular decision point in the cell death pathway [11]. The ratio of antagonist (Bcl-2, Bcl-x_L, Mcl-1, and A1) to agonist (Bax, Bak, Bcl-x_s, and Bad) molecules dictates whether a cell responds to a proximal apoptotic stimulus [11, 44–48]. Mitochondrial membrane permeabilization (MMP) can affect both the inner and outer mitochondrial membranes, which precedes the signs of necrotic or apoptotic cell death [49–51]. MMP is controlled mainly by the voltage-dependent anion channel (VDAC) and adenine nucleotide translocator (ANT), two of the most abundant proteins in the outer and inner membranes of the mitochondria. VDAC and ANT have also been shown to interact with the Bcl-2 family of proteins and to mediate mitochondrial damage during apoptosis [49–51]. In our system, mitochondrial damage and RGNNV-induced necrotic cell death were assessed in stable cell lines producing the anti-apoptotic Bcl-2 proteins, zfBcl-x_L or zfMcl-1a. Both zfBcl-x_L (Fig. 7(C):g and h) and zfMcl-1a (Fig. 7(C):e and f) strongly inhibited RGNNV-induced necrotic cell death (Fig. 7(C):c and d), reduced the percent of necrotic cells by up to 90% (zfBcl-x_L) and 93% (zfMcl-1a) at 36 h (Fig. 7(D); compare with the NNV-infected group) p.i., and correspondingly enhanced cell viability 102% (zfBcl-x_L) and 98% (zfMcl-1a) at 36 h (Fig. 7(E); compare with the RGNNV-infected group) p.i.

We schematically depict the steps to summarize the process of RGNNV-induced necrotic cell death (i.e., a newly synthesized protein(s) [necrotic death inducer] triggers the mitochondria-dependent death signal and then induces

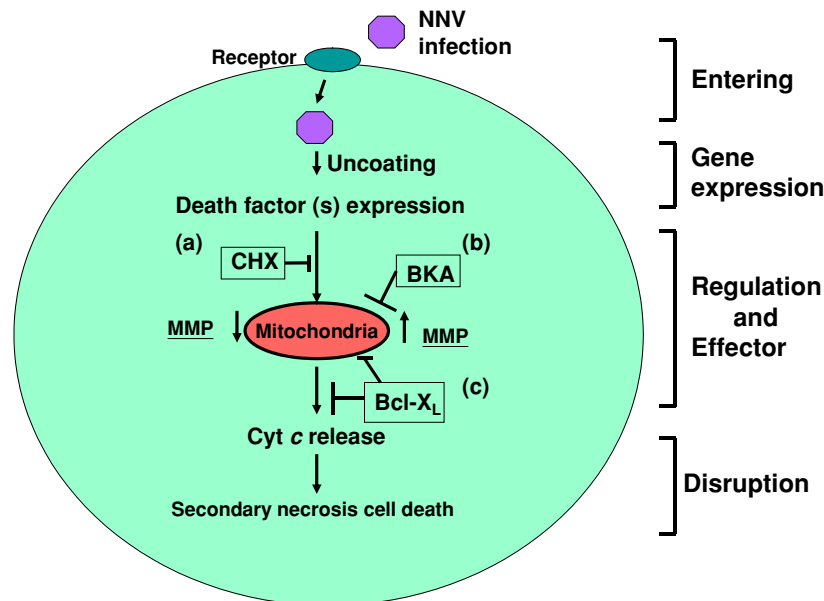


Fig. 9 The post-apoptotic necrosis cascade. The cell is exposed to a stimulus that is transmitted through the cellular machinery. For instance, RGNNV TN1 interacting with a cellular receptor may induce expression of a factor(s) encoded by a host cell gene or by early viral gene expression. In the effector stage, this necrotic factor may target mitochondria and induce loss of mitochondrial membrane potential (MMP) and subsequent release of mitochondrial cytochrome *c*. In the disruption stage, exposure of phosphatidylserine (PS) and endonuclease

alters the cytoskeleton, and DNA is restructured and cleaved before the cell body finally enters post-apoptotic necrosis. Necrotic factor expression (a) is blocked by the protein synthesis inhibitor CHX. A specific adenine nucleotide translocator (ANT) inhibitor of BKA (b) blocks mitochondrial permeability transition pore (MPTP) and the anti-apoptotic proteins, *xfBcl-x_L* and *xfMcl-1a*, and (c) prevents cytochrome *c* release by inhibiting cellular protease activation and PS exposure

cytochrome *c* release) and its inhibition by anti-Bcl-2 member proteins in Fig. 9.

Acknowledgments The authors are grateful to Dr. H. L. Yang (Institute of Biotechnology, National Cheng Kung University, Taiwan, ROC) for providing the grouper liver cell line (GL-av). This work was supported by grants (NSC-91-2311-B-006-007; NSC-92-2313-B-006-005) awarded to Dr. Jaiin-Ruey Hong from the National Science Council, Taiwan, Republic of China.

References

- Duvall E, Wyllie AH (1986) Death and the cell. *Immunol Today* 7:115–119
- Kerr JFR, Harmon BV (1991) Definition and incidence of apoptosis: an historical perspective. In: Tomei LD, Cope FO (eds) *Apoptosis: the molecular basis of cell death*. Cold Spring Harbor Laboratory Press, Cold Spring Harbor, pp 5–29
- Majno G, Joris I (1995) Apoptosis, Oncosis and necrosis: an overview of cell death. *Am J Pathol* 146:3–15
- Wang X (2001) The expanding role of mitochondria in apoptosis. *Genes Dev* 15:2922–2933
- Ferri KF, Kroemer G (2001) Organelle-specific initiation of cell death pathways. *Nat Cell Biol* 3:E255–E263
- Madesh M, Antonsson B, Srinivasula SM, Alnemri ES, Hajnoczky G (2002) Rapid kinetics of tBid-induced cytochrome *c* and Smac/DIABLO release and mitochondrial depolarization. *J Biol Chem* 277:5651–5659
- Adams JM, Cory S (1998) The Bcl-2 protein family: arbiters of cell survival. *Science* 281:1322–1326
- Antonsson B, Martinou JC (2000) The Bcl-2 protein family. *Exp Cell Res* 256:50–57
- McDonnell TJ, Beham A, Sarkiss M, Andersen MMP, Lo P (1996) Importance of the Bcl-2 family in cell death regulation. *Experientia* 52:1008–1017
- Farrow SN, Brown R (1996) New members of the Bcl-2 family and their protein partners. *Curr Opin Genet Dev* 6:45–49
- Van Regenmortel MHV, Fauquet CM, Bishop DHL et al (2000) *Virus taxonomy. Seventh report of the international committee on taxonomy of viruses*. Academic Press, San Diego
- Ball LA, Johnson KL (1999) Reverse genetics of nodaviruses. *Adv Virus Res* 53:229–244
- Nagai T, Nishizawa T (1999) Sequence of the non-structural protein gene encoded by RNA1 of striped jack nervous necrosis virus. *J Gen Virol* 80:3019–3022
- Nishizawa T, Mori K, Furuhashi M, Nakai T, Furusawa I, Muroga K (1995) Comparison of the coat protein genes of five fish nodaviruses, the causative agents of viral nervous necrosis in marine fish. *J Gen Virol* 76:1563–1569
- Schneemann A, Reddy V, Johnson JE (1998) The structural and function of nodavirus particles: a paradigm for understanding chemical biology. *Adv Virus Res* 50:381–446
- Johnson KN, Zeddum LL, Ball LA (2000) Characterization and construction of functional cDNA clones of pariacoto virus, the first alphanodavirus isolated Australasia. *J Virol* 74:5123–5132
- Li WX, Li HL, Lu R et al (2004) Interferon antagonist proteins of influenza and vaccinia viruses are suppressors of RNA silencing. *Proc Natl Acad Sci USA* 101:1350–1355
- Wnag XH, Aliyar R, Li WX et al (2006) RNA interference directs innate immunity against viruses in adult *Drosophila*. *Science* 312:452–454

19. Lu R, Maduro M, Li F et al (2005) Animal virus replication and RNA-mediated antiviral silencing in *Caenorhabditis elegans*. *Nature* 436:1040–1043
20. Li H, Li WX, Ding SW (2002) Induction and suppression of RNA silencing by an animal virus. *Science* 296:1319–1321
21. Sullivan CS, Ganem D (2005) A virus-encoded inhibitor that blocks RNA interference in mammalian cells. *J Virol* 79:7371–7379
22. Johnson KL, Price BD, Eckerle LD et al (2004) *Nodamura virus* nonstructural protein B2 can enhance viral RNA accumulation in both mammalian and insect cells. *J Virol* 78:6698–6704
23. Iwamoto T, Mise K, Takeda A et al (2005) Characterization of *striped jack nervous necrosis virus* subgenomic RNA3 and biological activities of its encoded protein B2. *J Gen Virol* 86:2807–2816
24. Fenner BJ, Thiagarajan R, Chua HK, Kwang J (2006) Betanodavirus B2 is an RNA interference antagonist that facilitates intracellular viral RNA accumulation. *J Virol* 80:85–94
25. Chen SP, Yang HL, Her GM et al (2006a) NNV induces phosphatidylserine exposure and loss of mitochondrial membrane potential in secondary necrotic cells, both of which are blocked by bongkrekic acid. *Virology* 347:379–391
26. Chen SP, Yang HL, Her GM et al (2006b) Enhanced viability of a nervous necrosis virus infected stable cell line over-expressing a fusion product of the zfBcl-xL and green fluorescent protein genes. *J Fish Dis* 29:347–354
27. Guo YX, Wei T, Dallmann K, Kwang J (2003) Induction of caspase-dependent apoptosis by betanodaviruses GGNNV and demonstration of protein α as an apoptosis inducer. *Virology* 308:74–82
28. Mori K, Nakai T, Muroga K, Arimoto M, Mushiaki K, Furusawa I (1992) Properties of a new virus belongs to nodaviridae found in larval striped jack (*Pseudocaranx dentex*) with nervous necrosis. *Virology* 187:368–371
29. Hong JR, Wu JL (2002) Induction of apoptotic death in cells via Bad gene expression by infectious pancreatic necrosis virus infection. *Cell Death Differ* 9:113–124
30. Verdier M, Malissein E, Munteanu E, Jayat-Vignoles C, Ratinaud M-H, Troutaud D (2006) Aged mice exhibit distinct peripheral B-cell phenotypes differing in apoptotic susceptibility: an Ex Vivo Anal. *Analyt Cytol* 69A:999–1009
31. Shimizu S, Matsuoka Y, Shinohara Y, Yoneda Y, Tsujimoto Y (2001) Essential role of voltage-dependent anion channel in various forms of apoptosis in mammalian cells. *J Cell Biol* 152:237–250
32. Laemmli UK (1970) Cleavage of structural proteins during the assembly of the head of bacteriophage T4. *Nature* 227:680–685
33. Kain SR, Mai K, Sinai P (1994) Human multiple tissue western blots: a new immunological tool for the analysis of tissue-specific protein expression. *BioTechniques* 17:982–987
34. McNulty MS, Connor TJ, McNeilly F, McLoughlin FM, Kirkpatrick KS (1990) Preliminary characterization of isolates of chicken anemia agent from the United Kingdom. *Avian Pathol* 19:67–73
35. Mullen PD, Brand RJ, Parlette GN (1975) Evaluation of dye exclusion and colony inhibition techniques for detection of polyoma-specific, cell-mediated immunity. *J Natl Cancer Inst* 54:229–231
36. Chipuk JE, Green DR (2005) Do inducers of apoptosis trigger caspase-independent cell death? *Nature Rev Mol Cell Biol* 6:268–275
37. Kroemer G, Martin SJ (2005) Caspase-independent cell death. *Nat Med* 11:725–730
38. Sorddet, O, Rébé C, Plenchette S, Zermati Y, Hermine O, Vainchenker W, Garrido C, Solary E, Dubrez-Dalozet L (2002) Specific involvement of caspases in the differentiation of monocytes into macrophages. *Blood* 100:4446–4453
39. Eckhart L, Declercq W, Ban J, Rendl M, Lengauer B, Mayer C, Lippens S, Vandenabeele P, Tschachler E (2000) Terminal differentiation of human keratinocytes and stratum corneum formation is associated with caspase-14 activation. *J Invest Dermatol* 115:1148–1151
40. Nakai T, Nguyen HD, Nishizawa T, Muroga K, Arimoto M, Otsuki K (1994) Occurrence of viral nervous necrosis in kelp grouper and tiger puffer. *Fish Pathol* 29:211–212
41. Cohen JJ, Duke RC, Fadok VA, Sellins KS (1992) Apoptosis and programmed cell death in immunity. *Annu Rev Immunol* 10:267–293
42. Ishid Y, Agata Y, Shibahara K, Honjo T (1992) Induced expression of the immunoglobulin gene superfamily, upon programmed cell death. *EMBO J* 11:3887–3895
43. Saelens X, Festjens N, Parthoens E et al (2005) Protein synthesis persists during necrotic cell death. *J Cell Biol* 168:545–551
44. Oltvai ZN, Millman CL, Korsmeyer SJ (1993) Bcl-2 heterodimerizes in vivo with a conserved homolog, Bax, that accelerates programmed cell death. *Cell* 74:609–619
45. Chittenden T, Harrington EA, Connor RO et al (1995) Induction of apoptosis by the Bcl-2 homologue Bak. *Nature* 374:609–619
46. Hunter JJ, Parslow TG (1996) A peptide sequence from Bax that converts Bcl-2 into an activator of apoptosis. *J Biol Chem* 271:7440–7444
47. Zha H, Aime-Sempe C, Sato T, Reed JC (1996) Proapoptotic protein Bax heterodimerizes with Bcl-2 and homodimerizes with Bax via a novel domain (BH3) distinct from BH1 and BH2. *J Biol Chem* 271:7440–7444
48. Yang E, Zha J, Jokel J, Boise LH, Thompson CB, Korsmeyer SJ (1995) Bad, a heterodimeric partner for Bcl-XL and Bcl-2, displaces Bax and promotes cell death. *Cell* 80:285–291
49. Marzo I, Brenner C, Zamzami N et al (1998) Bax and adenine nucleotide translocator cooperate in mitochondrial control of apoptosis. *Science* 281:2027–2031
50. Narita M, Shimizu S, Ito T et al (1998) Bax interacts with the permeability transition pore to induce permeability transition and cytochrome *c* release in isolated mitochondria. In: *Proc Natl Acad Sci USA* 95:14681–14686
51. Zamzami N, Kroemer G (2001) The mitochondrion in apoptosis: how Pandora's box opens. *Nature Rev Mol Cell Biol* 2:67–71